Princeton Plasma Physics Laboratory

PPPL-5249

Identification of multi-modal plasma responses to applied magnetic perturbations using the plasma reluctance

Nikolas C. Logan, Carlos Paz-Soldan, Jong-Kyu Park and Raffi Nazikian

May 2016

Prepared for the U.S. Department of Energy under Contract DE-AC02-09CH11466.

Princeton Plasma Physics Laboratory
Report Disclaimers

Full Legal Disclaimer

Trademark Disclaimer

PPPL Report Availability

Princeton Plasma Physics Laboratory:

http://www.pppl.gov/techreports.cfm

Office of Scientific and Technical Information (OSTI):

http://www.osti.gov/scitech/

Related Links:

U.S. Department of Energy

U.S. Department of Energy Office of Science

U.S. Department of Energy Office of Fusion Energy Sciences

Identification of Multi-Modal Plasma Responses to Applied Magnetic Perturbations using the Plasma Reluctance

Nikolas C. Logan[1], Carlos Paz-Soldan[2], Jong-Kyu Park[1], Raffi Nazikian[1]
[1]*Princeton Plasma Physics Laboratory, Princeton, New Jersey 08543, USA*
[2]*General Atomics, PO Box 85608, San Diego, CA 92186-5608, USA*

Using the plasma reluctance, the Ideal Perturbed Equilibrium Code (IPEC) is able to efficiently identify the structure of multi-modal magnetic plasma response measurements and the corresponding impact on plasma performance in the DIII-D tokamak. Recent experiments demonstrated that multiple kink modes of comparable amplitudes can be driven by applied nonaxisymmetric fields with toroidal mode number $n = 2$. This multi-modal response is in good agreement with ideal magnetohydrodynamic (MHD) models, but detailed decompositions presented here show the mode structures are not fully described by either the least stable modes or the resonant plasma response. This work identifies the measured response fields as the first eigenmodes of the plasma reluctance, enabling clear diagnosis of the plasma modes and their impact on performance from external sensors. The reluctance shows, for example, how very stable modes compose a significant portion of the multi-modal plasma response field and that these stable modes drive significant resonant current. This work is an overview of the first experimental applications using the reluctance to interpret the measured response and relate it to multifaceted physics, aimed towards providing the foundation of understanding needed to optimize nonaxisymmetric fields for independent control of stability and transport.

I. MOTIVATION

In tokamaks, nonaxisymmetric magnetic fields (δB) smaller than the axisymmetric field (B) by many orders of magnitude ($\delta B/B \sim 10^{-4}$) can drive energy, momentum, and particle transport, significantly impacting the plasma performance. Small asymmetries in the design and construction of tokamaks, inevitably create intrinsic error fields (EFs) of this order. Error field correction (EFC) coil sets are commonly used to negate any negative and/or amplify any positive consequence of the intrinsic error field. These intrinsic and applied external nonaxisymmetries drive the natural modes of the plasma, which can amplify or shield the perturbation relative to what it would have been in vacuum. The performance is then impacted by the effect of the total (external and plasma response) field on the physics of interest.

In the case of an unstable or marginally stable equilibrium, a single mode structure dominates the plasma response and that response dominates the total perturbation. This dominant mode can be directly probed using applied fields even when the intrinsic EF is unknown, and the plasma response resonant field amplification (RFA) used to optimize EFC to avoid instability[1–8]. These large marginally stable modes also modify equilibria of their own accord, and are used to control the momentum and density profiles of plasma[1,9–12]. The structure of this dominant mode and its driving external fields is calculable from an ideal magnetohydrodynamics (MHD) equilibrium, enabling predictive optimization of applied fields when direct experimental optimization is not available.

An intuitive description of natural modes of the system (plasma, surrounding vacuum, and possibly external current carrying structures) ranks the 3D perturbations in terms of their perturbed energy, δW. These are energy ranked eigenmodes of the equilibrium and form a complete orthonormal set of perturbations on the plasma surface in ideal MHD[13–15]. The ideal stability code DCON[15] calculates the energy eigenmodes of total surface displacement for a given axisymmetric equilibrium, the least stable of which indicates the proximity to instability. The marginally stable DCON mode is a good approximation of the dominant plasma response at or even slightly beyond the ideal MHD stability boundary and is used for active feedback resistive wall mode stabilization[16–20].

Separate from their role as indicators of approaching instabilities, large stable modes have significant impact of their own on the perturbed plasma equilibrium. The sheet current necessary to shield resonant components of the field in ideal MHD may be too great to sustain in practice, leading to reconnection, error field penetration, and the formation of islands. Even with flux surfaces intact, the stable perturbations may induce particle transport. Nonambipolar neoclassical transport across flux surfaces leads to the exchange of momentum between plasma and surrounding coils[21? –24], affecting stability through the rotation profile. Although the exact mechanism is still under study, stable resonant drive in the edge increases particle transport in the pedestal, reducing the pressure gradient and stabilizing edge localized modes (ELMs)[25–30].

In an effort to quantize the impact of these driven but stable modes, the Ideal Perturbed Equilibrium Code (IPEC) calculates a hierarchy of external perturbations ranked by the total resultant root-mean-square (RMS) resonant current drive (RCD) using singular value decomposition[4,31,32]. The singular values for a given toroidal mode number n decay exponentially, with the highest often an order of magnitude above the the second[33]. This implies that the resonant currents and correlated phenomena for that n can be well approximated by the extent to which any given external field overlaps

the first resonant coupling mode, and this overlap metric has been used extensively for predictive EFC[4,6,7,32,33].

Both the energy ranking and RCD ranking of perturbations can thus provide what is known as a single mode model, in which a single mode of perturbation determines the physics of interest. This reduction has been of primary importance for EFC, which typically uses little or no tuning of the applied poloidal spectrum to null a single mode component of the intrinsic EF[34,35]. The single mode model asserts that the rest of the spectrum, inevitably driven by such a coarse correction, is of negligible consequence.

Experiments at the DIII-D National Fusion Facility have demonstrated that intrinsic $n = 1$ EF correction currents are consistent with nulling the dominant RCD mode[7] and that the plasma is insensitive to $n = 1$ fields which have no overlap[6]. In such $n = 1$ experiments, the plasma response is dominated by the amplification of the first RCD coupled kink structure. This response then dominates the external magnetic measurements[36,37], making these measurement accurate metrics for the correction of the EF mode component.

In contrast to the $n = 1$ results, recent experiments have demonstrated that the plasma amplification of $n = 2$ EFs is multi-modal[38]. Changing the structure of the applied field excited multiple modes of plasma response to large amplitude. Despite this, the induced energy and particle (but not momentum) transport follows a single mode model with maxima/minima consistent with the coupling/decoupling of the external field to the first RCD ranked mode[9]. There is a discrepancy then, between the multi-modal amplitude of the externally measured plasma response and the single mode impact of the applied field on the equilibrium.

The discrepancy between the observed response and the equilibrium impact has important implications for multi-modal EFC and control, as the response amplitude measured by any given magnetic sensor array is no longer a good metric for EFC. In this paper, it will be shown that the observed response contains contributions from very stable and from nonresonant perturbations. This means neither a reduced set of the least stable modes nor the RCD modes can be used to efficiently interpret the measured response and relate it to the physics of interest.

The plasma reluctance eigenbasis succeeds were the aforementioned bases failed. The reluctance is a fundamental property of the axisymmetric plasma equilibrium that describes the effective perturbed currents that would arise if external fields drive nonaxisymmetry. It has hitherto remained a theoretical matter, unapplied in tokamak experiments and diagnostic analysis. The gaol of this paper is thus to introduce the plasma reluctance and show its initial applications in DIII-D. The applications show that the reluctance provides a framework for the interpretation of multi-modal measurements and means for relating them to the previous performance based metrics, enabling multi-modal control of the MHD response.

The organization of this paper is as follows. Section II reviews the experimental methods used at DIII-D to study $n = 2$ multi-modal plasma response and the impact of these multiple modes on the equilibria, highlighting the aforementioned discrepancy between the magnetic response and impact. Section III demonstrates the failure of the energy and RCD ranked field decompositions to describe the observed plasma response. A framework ranking applied fields by the external observability of their plasma response using the plasma reluctance is then introduced by Sec. IV. This framework efficiently describes the observed multi-modal response. Section IV provides the explicit relationship between the reluctance ranked modes and the two performance based decompositions. A discussion of the possible applications of this framework and final conclusions are in Sec. V.

II. EXPERIMENTAL MOTIVATION

The observation of multimodal plasma response to $n = 2$ fields has been detailed in many recent publications[10,30,38]. The plasma equilibria studied in these experiments are all ITER-similar shape lower single null plasmas as shown in Fig. 1 with toroidal field on axis of 1.93T. In all cases the structure of the applied field is changed by scanning the relative toroidal phase of 4kA $n = 2$ waveforms in two in-vessel coil arrays. Each coil array consists of six picture frame coils spanning sixty degrees in toroidal extent and with poloidal cross sections as shown in Fig. 1. Defining the kA current in the ith upper coil as $4\cos(n\phi_i - \phi_{IU})$ and in each lower coil as $4\cos(n\phi_i - \phi_{IL})$, the external field is parameterized by the phasing ($\Delta\phi_{UL} \equiv \phi_{IU} - \phi_{IL}$) of the upper relative to the lower coil set.

Figure 2 shows the Fourier decomposition in PEST[39] coordinates of the $n = 2$ external field structure at the plasma surface for the full range of phasings. The 300 and 0 degree phasing spectra both have nulls near the edge pitch resonant poloidal harmonic $m = 10 \sim nq_{lim}$ and peaks in the "kink resonant"[7,40] harmonics near $m = 15 \sim (n+1)q_{lim}$ that are often associated with the dominant plasma response in the single mode model. Indeed, these spectra excite the large multimodal responses observed in the experiment[38]. Here q_{lim} is defined as the safety factor of the IPEC control surface, which is necessarily just inside the last closed flux surface where q is finite.

The signature of multiple response structures in these experiments is the disparate $n = 2$ plasma response measured by magnetic sensors on the low-field-side (LFS) and high-field-side (HFS) of the vessel. Multi-modal response is defined by multiple structures of significant amplitude, leading to the measurements at these poloidal locations measuring different phasing dependences. Although this behavior has been observed[10] over a wide range of normalized plasma pressure (β_N), collisionality (ν_e^*), and total current (q_{95}), this paper will concen-

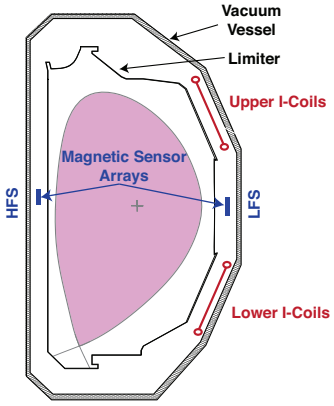

Figure 1. Cross section of the DIII-D tokamak, internal coils, magnetic sensor arrays, and ITER-similar shaped plasma used to study the multi-modal plasma response to $n = 2$ fields.

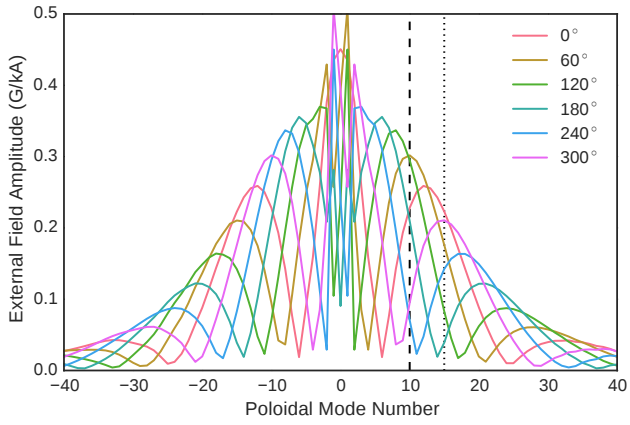

Figure 2. PEST coordinate poloidal spectra of the external field on the IPEC control surface applied by the I-Coils at 60° phasing intervals (indicated by color). The resonant pitch, nq_{lim}, near the surface containing 95% of the poloidal flux (dashed) as well as $(n+1)q_{lim}$ (dotted) vertical lines mark the nominal "pitch aligned" and "kink aligned" pitch.

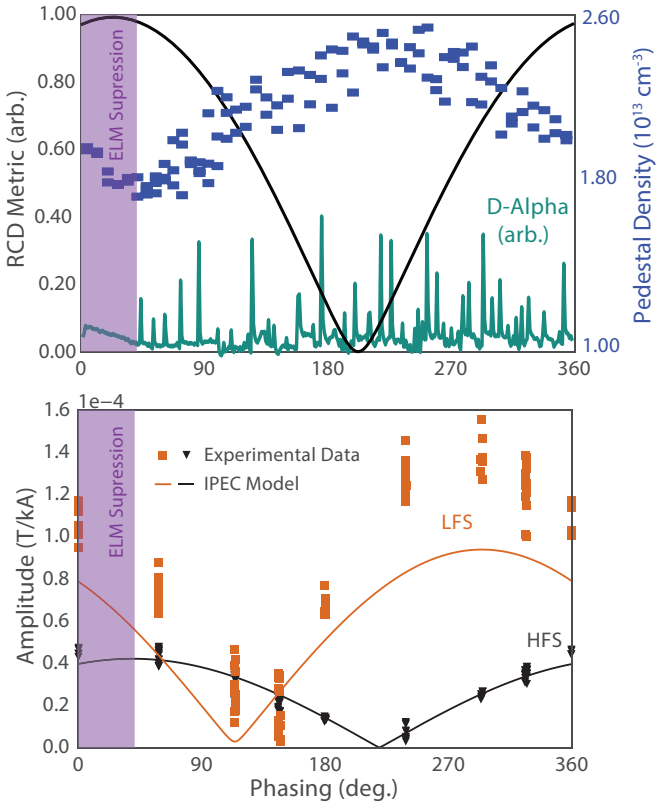

Figure 3. Top: The pedestal density (blue) and deuterium-α line emission from the divertor (green) as a function of I-coil phasing during a continuous experimental scan and dominant RCD mode metric for a IPEC modeled scan. Bottom: Discrete phasing $n = 2$ amplitude measurements from LFS (orange squares) and HFS (black triangles) magnetic sensor arrays and synthetic sensor signal predictions from IPEC (solid lines). Purple bands indicate phasings for which ELMs where suppressed. All data is as shown in Ref. [38].

trate on a reference equilibrium (158103) with $\beta_N = 2.2$, $\nu_e^* = 0.3$, and $q_{95} = 4.15$ unless otherwise specified. Reference [38] presented good agreement between the experimental measurements and ideal MHD modeling using IPEC for this scenario, both clearly showing multi-modal response. This agreement is reproduced in Fig. 3. Note that more complex resistive and extended MHD plasma response models, including MARS-F[41] and M3D-C^1[42], have also observed this behavior and have been benchmarked against IPEC in DIII-D[37]. This paper leverages the relative simplicity of the ideal MHD IPEC model to gain clear, physical insight into the experimentally observed behavior that is well described within its approximations.

Importantly, Ref. [38] showed that the energy transport as well as the particle transport and resulting ELM suppression were correlated with the coupling to the first RCD mode. This connection is further corroborated by the efficacy of single mode model EFC optimizing these metrics using the IPEC RCD metric in similar plasmas[9]. Note that despite the single mode behavior of the energy and particle transport, the momentum was decoupled from this RCD mode. It appears then that there are multiple large amplitude structures excited in the plasma and impacting the global equilibrium, but only one that induces the edge energy and particle transport that impact the ELMs.

It is desirable in experiments to interpret the importance of an external magnetic measurement in terms of its implied performance impact. A prime example is the $n = 1$ LFS plasma response amplitude, which has been successfully used to indicate proximity to stability boundaries and the amount of induced transport in single mode EFC experiments[43,44]. With multi-modal responses it is not possible to draw a direct connection between the observed signal and physics of interest. Certainly, the nulling the LFS signal does not minimize the impact of the applied field in Fig. 3. An understanding of

which modes of response are observed by external magnetic sensors as well as which are meaningful for performance is necessary to accurately interpret impact from measurements.

III. IDENTIFICATION USING PLASMA PERFORMANCE BASES

This section describes the energy ranked and RCD ranked external field perturbations on the plasma surface as computed by the ideal MHD codes DCON[15] and IPEC[31]. Both codes use a formalism in which nonaxisymmetric flux surface perturbations are expressed to arbitrary accuracy using Fourier decomposition in angular magnetic coordinates (ϑ, φ). Perturbations of different toroidal mode numbers (n) are decoupled by symmetry and are treated independently in the codes. For a given n, any nonaxisymmetric quantity $V(\vartheta, \varphi)$ on the flux surface ψ can be written as the column vector,

$$\boldsymbol{V}(\psi) = \{V_m(\psi),\ m_{min} \leq m \leq m_{max}\}, \tag{1}$$

where V_m is the Fourier coefficient of the angular function for poloidal mode number m.

This formalism can be used to compactly describe a wide range of both time independent and time dependent phenomena relating nonaxisymmetric fields and toroidal plasma confinement with matrix equations intuitively similar to those of circuit theory[14]. The DCON and IPEC codes, however, focus on time independent perturbed equilibria.

The direct criterion of Newcomb (DCON) code calculates the stability of nonaxisymmetric perturbations about an axisymmetric equilibrium[15,45]. The code calculates solutions of a high order Euler-Lagrange system of ordinary differential equations, describing the displacements of flux surfaces that minimize the ideal MHD perturbed energy. The minimization of the perturbed energy $\delta W = \int dx^3 \boldsymbol{\xi} \cdot F(\boldsymbol{\xi})$ with respect to the nonaxisymmetric displacement $\boldsymbol{\xi}$ provides M orthogonal ideal MHD force (F) balance solutions for which $F(\boldsymbol{\xi}) = 0$. Here, M is the number of poloidal harmonics retained in the calculation. The M solutions span the space of all valid ideal MHD perturbed equilibria for a given n and m truncation.

All of these perturbed equilibria are uniquely defined by their displacement, or alternatively their flux, on the outermost surface of the computational domain (q_{lim}) approaching the surface of the plasma. And the total energy of an arbitrary perturbation on this surface is,

$$\delta W = \boldsymbol{\Phi}^{\dagger} \cdot \boldsymbol{\Lambda}^{-1} \cdot \boldsymbol{\Phi}, \tag{2}$$

where the inverse plasma inductance, $\boldsymbol{\Lambda}^{-1}$, is calculated directly by the minimization done in DCON. In ideal MHD, the inverse plasma inductance is a hermitian matrix. The eigenvectors $\boldsymbol{\Phi}_i$ of this matrix thus provide a complete, orthonormal basis set ordered by eigenvalues representing the perturbed energy per square unit total flux.

In a stable plasma, each of these eigenmodes has a positive eigenvalue and must be externally driven in order to be physically realized. The ideal perturbed equilibrium code (IPEC) calculates the perturbed flux $\boldsymbol{\Phi}$ given an applied external flux, $\boldsymbol{\Phi}_x$, using the linear relationship,

$$\boldsymbol{\Phi} = \boldsymbol{\Lambda} \cdot \mathbf{L}^{-1} \cdot \boldsymbol{\Phi}_x. \tag{3}$$

Here the control surface inductance $\mathbf{L}$ defines the flux on the surface produced by a surface current $(\mathbf{I})$ such that $\boldsymbol{\Phi} = \mathbf{L} \cdot \mathbf{I}$, and the plasma inductance relates the total flux to an effective surface current of the external field $\boldsymbol{\Phi} = \boldsymbol{\Lambda} \cdot \mathbf{I}_x$. Given an external flux, IPEC solves for the total flux using Eq. (3) and decomposes it in the DCON eigenbasis such that $\boldsymbol{\Phi} = \sum_{i=1}^{M} c_i \boldsymbol{\Phi}_i$. The perturbed equilibrium is then fully defined at any point $(\psi, \vartheta, \varphi)$ in the plasma as the similarly weighted sum of DCON force balance solutions.

The following sections discuss, in detail, various ways in which the external perturbations applied in IPEC can be categorized by the physics of interest. The conclusion demonstrates the power of the full eigenmode calculation in constructing reduced models for understanding the experiment and the physics. Note that while many codes are used to compute the driven nonaxisymmetric plasma response in DIII-D[37], at this time only DCON and IPEC formulate the complete eigenbasis of the input axisymmetric equilibrium independent of external drive. More complex models, often calculate a single least stable plasma mode by running time dependent calculations with white noise initial conditions of nonaxisymmetry. Time independent 3D equilibrium calculations, however, have historically concentrated on calculating only the explicitly driven response. There is no fundamental reason the eigenmodal descriptions presented here could not include physics beyond that of ideal MHD, although the extension of the IPEC formalism to a Generalized Perturbed Equilibrium Code (GPEC)[46] is beyond the scope of this paper. Here, we use the ideal MHD results, which agree well with the experimental observations, to motivate the basic plasma property classifications of multimodal plasma responses that may be extended to include more physics as it is motivated by observations in other experimental regimes.

A. Energy Gain Ranked Eigenspace

The eigen decomposition of the inverse plasma inductance in DCON is an intuitive and informative categorization. Any negative eigenvalue immediately implies ideal instability. A marginally stable eigenmode is a good approximation of the unstable resistive wall mode structure[16,17,20] and can reasonably be expected to dominate any perturbed equilibrium. A marginally stable mode is defined as one for which the perturbed

energy (δW) is much smaller than the energy required to similarly perturb the vacuum (δW_v) such that $s = -\delta W/\delta W_v \to 0$. Note that s is defined by the ratio of two scalars,

$$s = -\frac{\delta W}{\delta W_v} = -\frac{\mathbf{\Phi}^\dagger \cdot \mathbf{\Lambda}^{-1} \cdot \mathbf{\Phi}}{\mathbf{\Phi}^\dagger \cdot \boldsymbol{L}^{-1} \cdot \mathbf{\Phi}}, \tag{4}$$

and does not provide a eigenbasis of its own. The "least stable kink", however, is given by the smallest eigenvalue and corresponding eigenvector of $\mathbf{L} \cdot \mathbf{\Lambda}^{-1}$ in stable equilibria by virtue of both matrices being positive definite.

The experimental results detailed in the previous section, however, show more than one external field excites a large plasma response. This equilibrium is, and the majority of DIII-D plasmas are, relatively far from any $n > 1$ ideal MHD stability boundary where the least stable mode would be expected to dominate over all others. In such cases, a multimodal eigenbasis is required to describe the perturbed equilibrium, ruling out the stability ranking discussed above that gives only the least stable mode. A natural evolution is to rank the external field structures by the energy of the total perturbation they produce.

The energy of a perturbed equilibrium driven by external coils can be written in terms of the control surface external flux by combining Eqs. (2) and (3),

$$\delta W = \mathbf{\Phi}_x^\dagger \cdot \mathbf{L}^{\dagger -1} \cdot \mathbf{\Lambda} \cdot \mathbf{L}^{-1} \cdot \mathbf{\Phi}_x. \tag{5}$$

This work, following the energy normalization used in Ref. [4], will use a square-root area weighted field vector $\tilde{\mathbf{\Phi}}_x$ with components Φ_m such that,

$$\sqrt{\mathcal{J}\,|\nabla\psi|}B^{norm} = \sum_{m=m_{min}}^{m_{max}} \tilde{\Phi}_m(\psi) e^{-i(m\theta - n\phi)}. \tag{6}$$

Here B^{norm} is the normal field on the surface. The L-1 norm,

$$\tilde{\mathbf{\Phi}}_x \cdot \tilde{\mathbf{\Phi}}_x = \int d\vartheta d\varphi \mathcal{J}\,|\nabla\psi|\,(B^{norm})^2\,, \tag{7}$$

is proportional to the line energy of the applied external field and for the remainder of this paper this quantity will be referred to as the e-flux. The e-flux is related to the true flux by the hermitian weighting matrix $\mathbf{W}$, such that $\mathbf{\Phi}_x = \mathbf{W} \cdot \tilde{\mathbf{\Phi}}_x$.

The perturbed equilibrium energy expressed in the e-flux basis is given by,

$$\delta W = \tilde{\mathbf{\Phi}}_x^\dagger \cdot \mathbf{G} \cdot \tilde{\mathbf{\Phi}}_x, \tag{8}$$

where the energy gain matrix $\mathbf{G} = \mathbf{W}^\dagger \cdot \mathbf{L}^{\dagger -1} \cdot \mathbf{\Lambda} \cdot \mathbf{L}^{-1} \cdot \mathbf{W}$ is again a hermitian matrix. The eigenvalues of this matrix are proportional to the perturbed equilibrium energy per unit line energy in the external field at the plasma surface, and corresponding eigenvectors form a complete orthonormal basis in which any external field can be decomposed. The precise eigenvalues and eigenvectors that compose the bases are fundamental properties of the axisymmetric equilibrium.

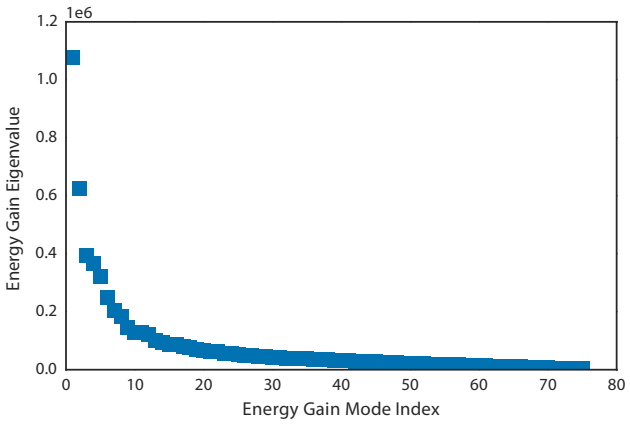

Figure 4. The energy gain matrix eigenvalues for the multimodal reference equilibrium.

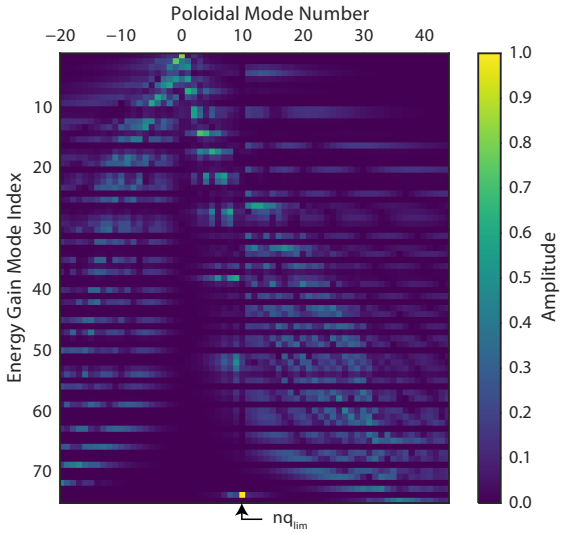

Figure 5. The energy gain matrix eigenvectors (rows) sorted on the vertical axis from largest (top) to smallest (bottom) eigenvalue. The amplitudes of each row sum to unity (the eigenvectors are unit vectors).

Figures 4 and 5 show the eigenvalues and eigenvectors of the energy gain matrix for the equilibrium modeled in Sec. II. The Fourier space was truncated such that $-20 \leq m \leq 44$, and there are correspondingly 75 unique eigenmodes. The eigenvalues fall rapidly, indicating a small number of modes determine the total perturbed energy. The highest eigenvalue modes are concentrated near the lowest magnitude poloidal harmonics, with some contribution from the "kink aligned" harmonics near $m \sim 12$. The lowest eigenvalues correspond to eigenvectors that are spread across high Fourier harmonics, with the notable exception of a few modes sharply peaked near $m = 10$, which corresponds to the pitch of

the last rational surface contained within the computational domain. This pitch resonant mode is extremely difficult to drive.

The applied fields, shown in Fig. 2, are predominantly composed of the lower ($|m| < 20$) poloidal wavenumber components. Any applied spectrum $\tilde{\mathbf{\Phi}}_x$ can be decomposed in the gain ranked eigenmodes $\tilde{\mathbf{\Phi}}_{\substack{x\\G\\i}}$. Figure 6 shows the applied spectra decomposed in the stability basis, confirming that all phasing couple best to the low m, large eigenvalue modes. Still, there is significant drive for the few stable modes mentioned above with the edge rational pitch.

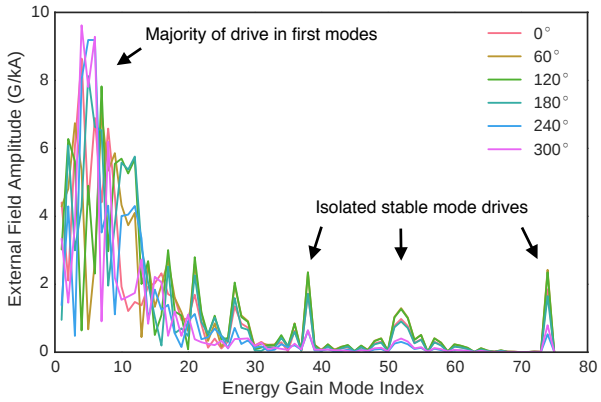

Figure 6. Energy gain eigenbasis decomposition of the external field on the IPEC control surface applied by the I-Coils at 60° phasing intervals (indicated by color).

The contribution of each gain ranked eigenmode to the measured plasma response can be calculated by isolating the projection of the true external field on one or multiple eigenmodes. If a small number of basis functions closely approximates the observed response, these modes might be constrained by a practical number of external magnetic measurements and thus be usable for active feedback stability control. Figure 7 shows the synthetic sensor signal as a function of phasing cumulatively including the isolated contribution of each eigenmode from the smallest to largest eigenvalue. The average χ^2 error in the top plot shows that that the synthetic LFS sensor signal converges regularly but slowly as the number of modes is increased. The HFS signal contains a significant contribution from the driven low gain modes discussed before, resulting in poor convergence and significant discrepancies even with nearly the full number of eigenmodes.

The somewhat counterintuitive result that these highly stable modes contribute significantly to the measured plasma response effectively negates using the high gain eigenmodes to succinctly describe said response. This means the few modes that determine the total perturbed energy of the plasma cannot, on their own, be used to in-

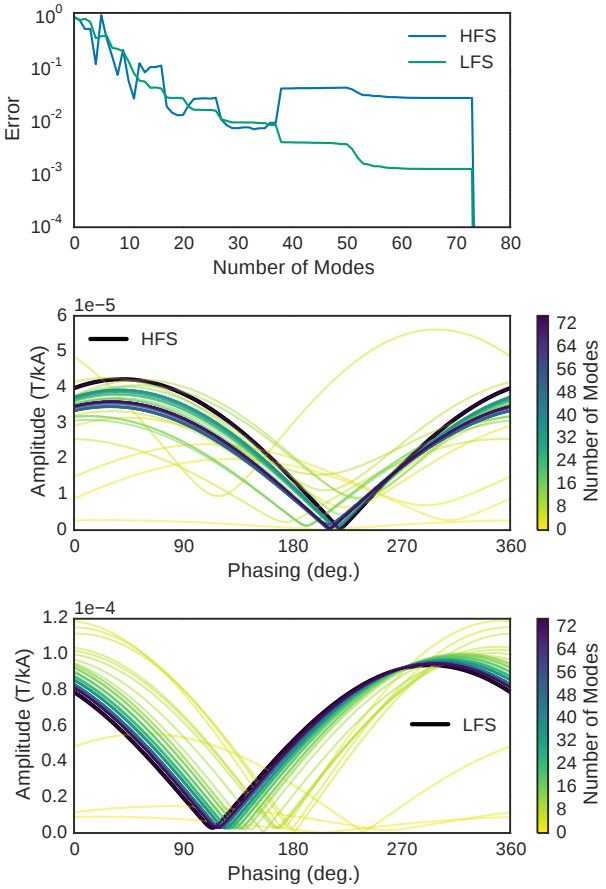

Figure 7. Top: Relative error of the HFS (blue) and LFS (green) magnetics signal produced by isolating a cumulative number of energy gain eigenmodes. Middle: The full HFS signal (black, bold) calculate by IPEC and the cumulative contributions of progressively larger numbers (indicated by color) of eigenmodes. Bottom: The corresponding full and partial signals for the LFS sensors.

terpret and feedback on the measured plasma response. Feedback might lead, for example, to unnecessary "suppression" of the very stable modes. Since experimental identification of all M eigenmodes is impractical, a separate identification of the plasma response measurements is thus needed before they can be confidently related to the impact of applied fields on the perturbed energy.

B. Resonant Coupling Ranked Space

A second common ranking metric for the impact of a perturbation on the equilibrium is the associated resonant current drive (RCD). This metric has been used extensively in EFC efforts in active machines[4–7], as well as for the prediction of EF thresholds for future devices such as NSTX-U and ITER[33,47]. The premise behind this metric is that the surface current required to shield resonant ($m = nq$) flux in ideal MHD is indicative of the

drive for islands at rational surfaces and that the opening of these islands -not necessarily the global mode stability- is the largest direct impact of the external fields on the equilibrium. This impact has historically been the advent of EF penetration for $n = 1$, while external perturbation with $n = 2$ and 3 have been linked to ELM suppression through the formation of islands at the top of the edge pedestal formed in H-mode plasmas[29,30]. Despite the disparate physics at island formation, the IPEC RCD metric has been successful in predicting the optimal application of external fields to inhibit or drive mode locking and ELM suppression[6,7,10,38].

Within the linear ideal MHD framework of IPEC, the resonant current on each rational surface in the computation domain is linearly related to the external e-flux such that,

$$\tilde{\mathbf{I}}_r = \boldsymbol{\mathcal{C}} \cdot \tilde{\boldsymbol{\Phi}}_x. \tag{9}$$

Here $\tilde{\mathbf{I}}_r$ is a $R \times 1$ matrix vector of the square-root area weighted resonant current at each rational surface, $\tilde{\boldsymbol{\Phi}}_x$ is again the $M \times 1$ external e-flux vector, and $\boldsymbol{\mathcal{C}}$ is a $R \times M$ coupling matrix. Here R is the number of rational surfaces within the computational domain, and $\mathcal{C}_{rm}$ is the coupling between each applied poloidal harmonic m and rational surface r. The coupling matrix is, in general, not square and not hermitian. It is, however, positive definite, and decomposing the matrix using singular value decomposition gives R positive singular values c_r. These singular values rank the corresponding unit right singular vectors of external e-flux by the RMS power of induced resonant currents $\sum_r \int d\vartheta d\varphi \mathcal{J}_r |\nabla\psi|_r I_r^2$. These modes do not form a complete basis with which any external e-flux $\tilde{\boldsymbol{\Phi}}_x$ can be decomposed. They do, however, form a unit basis of the e-flux spanning the full space for which there is any resonant current drive from external fields. The first of these modes has been called the *dominant external field*[4,33], dominant mode[6,7] or just SVD1[38]. This work does not restrict its focus to one mode, but considers the entire resonant current driving right singular basis referred to henceforth simply as the RCD modes.

Figures 8 and 9 show the resonant coupling singular values and corresponding RCD modes for the equilibrium studied in Sec. II. There are eight rational surfaces ($R = 8$) within the computational domain extending from 0.001 to 0.987 in normalized poloidal flux, and thus eight singular values. These singular values decrease exponentially, with one mode dominating the resonant current power. This dominant mode is localized in Fourier space near the "kink resonant" harmonics $m \sim 12$, while subsequent modes peak at progressively lower poloidal mode numbers. These sub-dominant modes drive more core localized modes, the large wavelength of which easily create large signals on the LFS sensor. The RMS current drive ranking preferentially weights modes towards the edge, where the $n = 2$ rational surfaces are closely packed. Despite these subtleties, all the RCD modes are concentrated in a relatively compact range of poloidal mode numbers between 4 and 12. As consequence of this concentration, the fields applied in the experimental phasing scan contain significant drive for all the RCD modes.

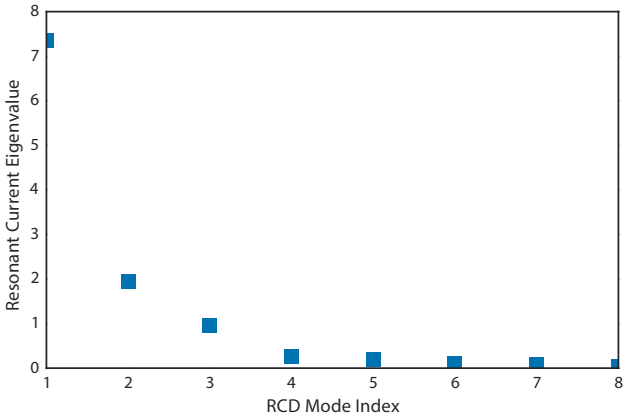

Figure 8. The RCD matrix singular values for the multi-modal reference equilibrium.

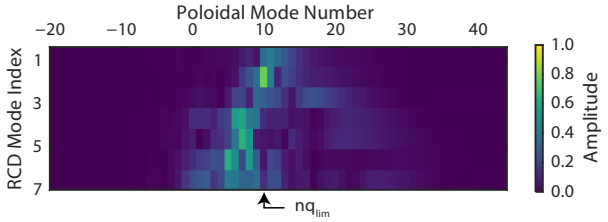

Figure 9. The 8 RCD matrix right singular vectors (rows) sorted on the vertical axis from largest (top) to smallest (bottom) singular value. The amplitudes of each row sum to unity (the vectors are unit vectors).

The RCD basis is a significant reduction of the external e-flux space that efficiently isolates and captures the drive for resonant physics. As such, it is a powerful tool for predictive optimization of external fields in multi-modal plasmas when the resonant response dominates the impact. As reported in Refs. [38] and [9], the coupling of the external field to the dominant RCD mode is correlated with ELM suppression and with the energy and density pump-out, which have single mode model dependencies on the phasing despite the multi-modal plasma response.

The multi-modal nature of the measured response, however, makes it difficult to assess the RCD coupling without performing a full perturbed equilibrium calculation. This is evident in the fact that the coupling metric reported in Ref. [38], and reproduced in Fig. 3, is not perfectly correlated with either the LFS or HFS amplitudes. It is more correlated with the HFS than LFS, which suggests the hypothesis that the HFS amplitude is dominated by the resonant response and could be a experimental metric for optimizing the applied fields for ELM suppression.

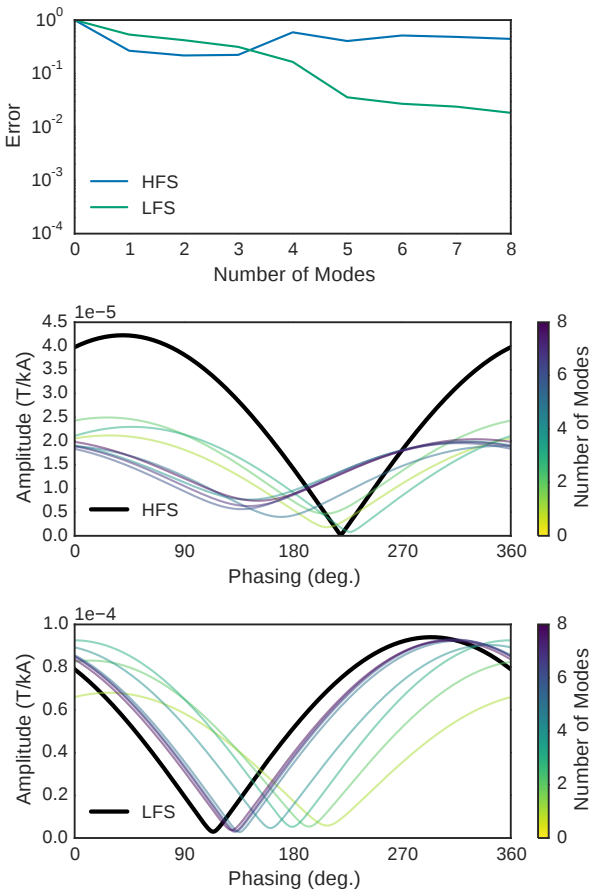

Figure 10. Top: Relative error of the HFS (blue) and LFS (green) magnetics signal produced by isolating a cumulative number of RCD modes. Middle: The full HFS signal (black, bold) calculate by IPEC and the cumulative contributions of all 8 (indicated by color) RCD modes. Bottom: The corresponding full and partial signals for the LFS sensors.

This hypothesis that the HFS signal is dominated by the resonant response is, unfortunately, disproven by isolating the RCD mode contributions to the calculated perturbed equilibrium. Figure 10 shows the synthetic sensor signal as a function of phasing cumulatively including the isolated contribution of each RCD mode from the largest to smallest singular value. Including all eight RCD modes includes the entirety of resonant current drive from the external fields throughout the phasing scan. Counter to the speculation of preferential HFS sensitivity to the resonant response, Fig. 10 shows that the amplitude of the HFS signal is not recovered when including the full resonant response. The remaining HFS signal must be coming from the components of the external field driving completely nonresonant perturbations. The LFS, despite disparate dependence on the phasing, contains a large contribution from the first mode. Its synthetic signal quickly converges to a good approximation of its value in the full perturbed equilibrium calculation: matching the maxima phasing within 16° and amplitude within 2% of it's full value.

Active control of the resonant current drive physics of interest using external magnetic sensors is ambiguous from the RCD coupling basis description alone. The LFS signal is composed almost entirely of the resonant response, but is a combination of all the edge and core modes obscuring the dominant RCD mode needed to optimize for edge density transport or ELM suppression. The HFS signal is amplified by a similar external field structure as that best coupled to the dominant RCD mode, but is not composed of the response to that mode alone. It is sensitive to an additional nonresonant response, outside of and not described by the RCD modes. Neither measurement, then, can be generally extrapolated as a metric for optimization of ELM control in new equilibria or machines.

IV. IDENTIFICATION USING A PLASMA RESPONSE FIELD BASIS: THE PLASMA RELUCTANCE EIGENSPACE

This section presents an alternative basis of external fields derived from and ranked by the plasma reluctance. The reluctance, $\boldsymbol{\rho}$, is a property of the plasma long since identified[1,14,34,48] but little used in application. It describes the degree of difficulty with which one can pass a magnetic field through the plasma. In the control surface matrix-vector framework of IPEC, the reluctance defines the linear relationship between the effective perturbed surface current, $\boldsymbol{\mathcal{I}}_p$, required to describe the plasma response field outside the plasma and the external flux,

$$\boldsymbol{\mathcal{I}}_p = \boldsymbol{\rho} \cdot \boldsymbol{\Phi}_x, \tag{10}$$

and can be written in terms of the plasma and surface inductance as,

$$\boldsymbol{\rho} = \mathbf{L}^{-1} \cdot \left(\boldsymbol{\Lambda} \cdot \mathbf{L}^{-1} - 1 \right). \tag{11}$$

Here the surface current, $\boldsymbol{\mathcal{I}}_p$, is a virtual current that can be used to uniquely define the field outside the surface produced by perturbed currents throughout the plasma volume.

The energy normalized current and flux used in the previous sections are related to each other by,

$$\tilde{\boldsymbol{\mathcal{I}}}_p = \boldsymbol{\varrho} \cdot \tilde{\boldsymbol{\Phi}}_x, \tag{12}$$

where the normalized reluctance,

$$\boldsymbol{\varrho} = \mathbf{W} \cdot \boldsymbol{\rho} \cdot \mathbf{W}, \tag{13}$$

is again a Hermitian matrix. The eigenvectors of this matrix span the complete space of external e-flux and are ranked according to the effective plasma current power per unit line energy of external field.

The reluctance basis is arguably the best physics basis with which to rank modes by their observability on external magnetics. These measurements are of the flux through a diagnostic coil, Φ_d, which is linearly coupled

to the effective surface current by a mutual inductance $\mathbf{M}_{dp}$ such that the plasma response measurement is,

$$\mathbf{\Phi}_d = \mathbf{M}_{dp} \cdot \boldsymbol{\mathcal{I}}_p = \mathbf{M}_{dp} \cdot \mathbf{W} \cdot \boldsymbol{\varrho} \cdot \tilde{\mathbf{\Phi}}_x. \tag{14}$$

Here the the mutual inductance and area weighting matrices are fully determined by the geometry of the sensor and plasma surface and do not depend on the plasma physics. They are specific to every machine and diagnostic system. The reluctance, however, contains the plasma physics that determines whether or not there will be any observable magnetic response outside the plasma for a given external field.

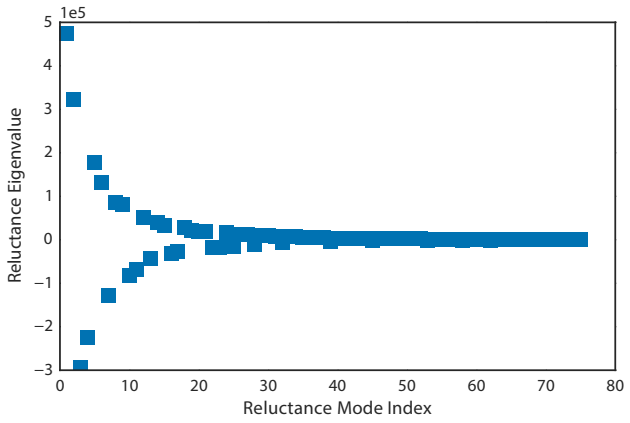

Figure 11. The reluctance matrix eigenvalues for the multimodal reference equilibrium.

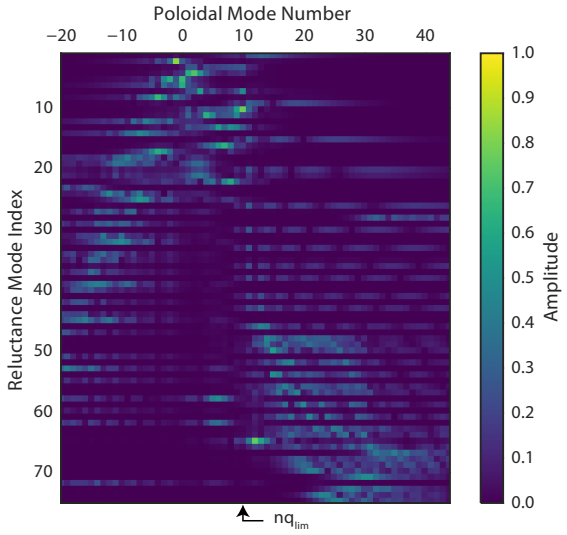

Figure 12. The reluctance matrix eigenvectors (rows) sorted on the vertical axis from largest (top) to smallest (bottom) eigenvalue. The amplitudes of each row sum to unity (the eigenvectors are unit vectors).

Figures 11 and 12 show the eigenvalues and eigenvectors of the reluctance matrix $\boldsymbol{\varrho}$ for the equilibrium modeled in Sec. II. The eigenvalues are positive and negative. The squared values give the effective current power per unit energy in the external field on the control surface, which is related to the energy in the diagnostic coils as discussed above. For positive eigenvalues, the effective current of the corresponding eigenmode is in phase with the external field, and the plasma amplifies the field. Reluctance eigenmodes with negative eigenvalues have effective currents in the opposite direction, diminishing the external magnetic field.

Figure 13 shows the isolated first two (most positive) and following two (most negative) reluctance eigenmode components of the external field produced by 0° phasing and the resulting perturbed equilibrium fields at the control surface if only these modes were applied. The two positive modes are the two first modes shown in figures 11 and 12, and their linear combination will provide the synthetic diagnostic signal for the first two modes as before. The next two reluctance eigenvalues are negative, and their corresponding external e-flux eigenvectors have been similarly combined before calculating the corresponding perturbed equilibrium. The final field is clearly larger than the applied field in the case of the positive eigenvalue modes and lower than the applied field in the case of the negative eigenvalues. This is a clear demonstration of the amplifying/shielding dichotomy. These extrema and the other eigenmodes of large magnitude reluctance are predominantly composed of low magnitude poloidal mode numbers within the range of the applied fields from the experimental phasing scan. These longer wavelength modes are also the most likely to be measured by external magnetics displaced radially from the plasma (the field would fall off as Δr^{-m} in a cylinder) as well as the fields thought to be of the most physical importance (see, for example the dominant modes of the previous section).

The poloidal Fourier spectra for these two amplifying and two shielding modes are shown explicitly in Fig. 14. Again, the amplification/shielding of the external field (dashed lines) is readily apparent. The modes amplified are concentrated in the usual kink resonant harmonics ($m \gtrsim nq_{95}$) mentioned in previous sections, while the shielding modes encompass a spread of poloidal harmonics from very low to pitch-resonant m. Interestingly, both amplifying and shielding modes contain significant low magnitude poloidal harmonics with the opposite helicity as that of the equilibrium field lines. These contributions are purely nonresonant and the resulting plasma response would thus not be captured by, for example, the RCD modes.

Figure 15 shows that the reluctance eigenmodes efficiently describe the observed plasma response for the equilibrium modeled in Sec. II. The plots, like those of the previous section, show the sensor signal from the full perturbed equilibrium and perturbed equilibria isolating the response to a cumulative number of eigenmodes. Here, reluctance eigenmodes are used in order of their eigenvalue magnitude. Unlike the previous sections, the

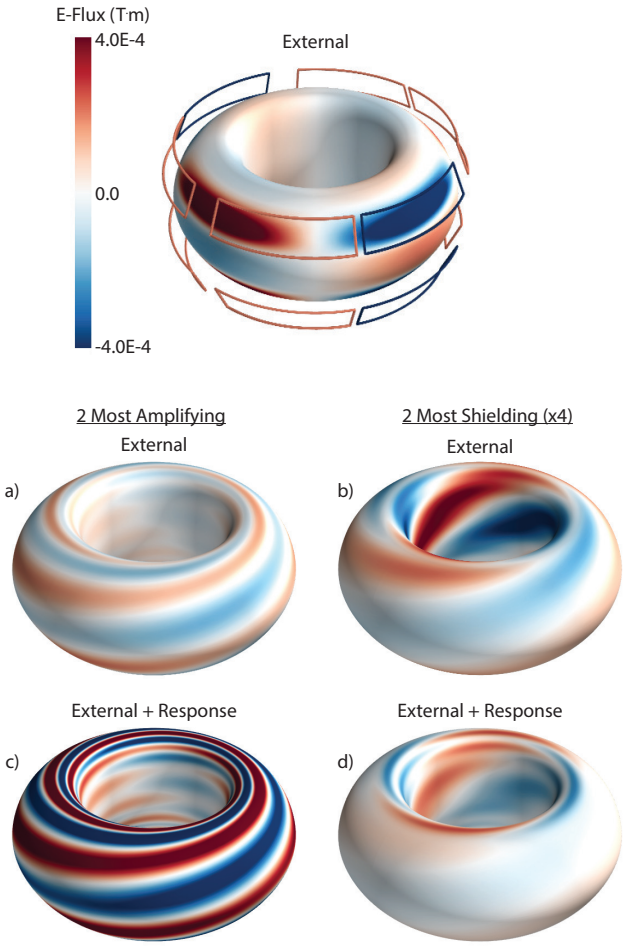

Figure 13. The e-flux applied on the IPEC control surface using 1kA $n = 2$ I-coil waveforms with zero degree phasing (top) and the isolated components aligned with the largest two positive eigenvalue modes combined (a) and largest two negative eigenvalue modes combined (b). The perturbed equilibrium e-flux calculated using only the isolated positive (c) and negative (d) eigenvalue drives show amplification and shielding of the driving e-flux respectively.

relative error between the full and isolated signals quickly decreases for both the HFS and LFS sensor arrays. Using only 8 reluctance eigenmodes to describe the applied field, the HFS(LFS) signal maxima are matched within 13(18) degrees and 3(9)% of their full magnitude. That this convergence should take place for an ideal sensor set follows from the very definition of the reluctance, but Fig. 15 is the first application of the reluctance eigenbasis for describing actual sensor data in a real tokamak with complete experimental geometry.

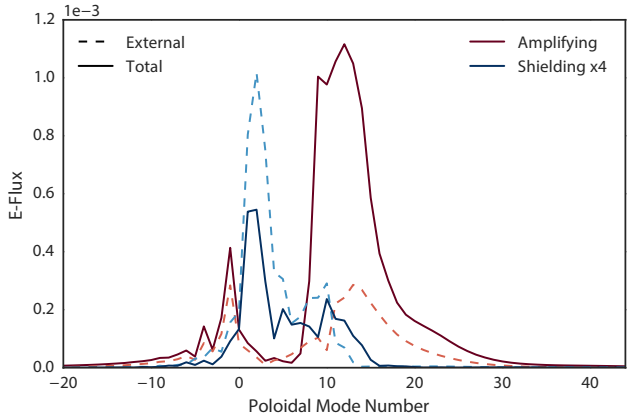

Figure 14. The poloidal spectrum of the largest two positive eigenvalue modes combined (red) and largest two negative eigenvalue modes combined (blue) isolated from the applied zero degree phasing (dashed) and the corresponding perturbed equilibrium (solid) showing amplification and shielding respectively.

A. Relation between the Reluctance and Performance Ranked Bases

This section has shown that the reluctance succeeds where previous metrics failed to efficiently describe the plasma response measured by magnetic sensors external to the plasma. The previously prevalent metrics are, however, still of great relevance to the performance of the plasma in the presence of 3D perturbations. This section thus details the relationship between the reluctance and the stability and RCD bases.

The reluctance is rigorously related to the stability by Eq. (11). In a single mode model, the reluctance and each of its composite matrices can be reduced to scalars such that,

$$\rho L = -\frac{1+s}{s}. \tag{15}$$

Here $s = -\delta W/\delta W_v$ is the common stability metric used previously. Two features of this relationship are immediately apparent. First, in the marginal stability limit $s \to 0$ the reluctance approaches infinity asymptotically as $-1/s$. This says that the reluctance of a plasma will be dominated by the marginally stable mode as the plasma approaches the stability boundary for a given n. Second, very stable modes with $-s \gg 1$ contribute finite negative reluctance. These are the shielding modes discussed above, and the lower bound of -1 in Eq. (15) an expression of the fact that the plasma will never "shield" more flux than is applied. In this infinitely stable limit, the plasma acts like a superconductor and perfectly shields the applied flux at the control surface.

In any true tokamak equilibrium, the full matrices of Eq. (11) couple multiple modes together and analysis is not quite as clean. Even in the clearly multi-modal plas-

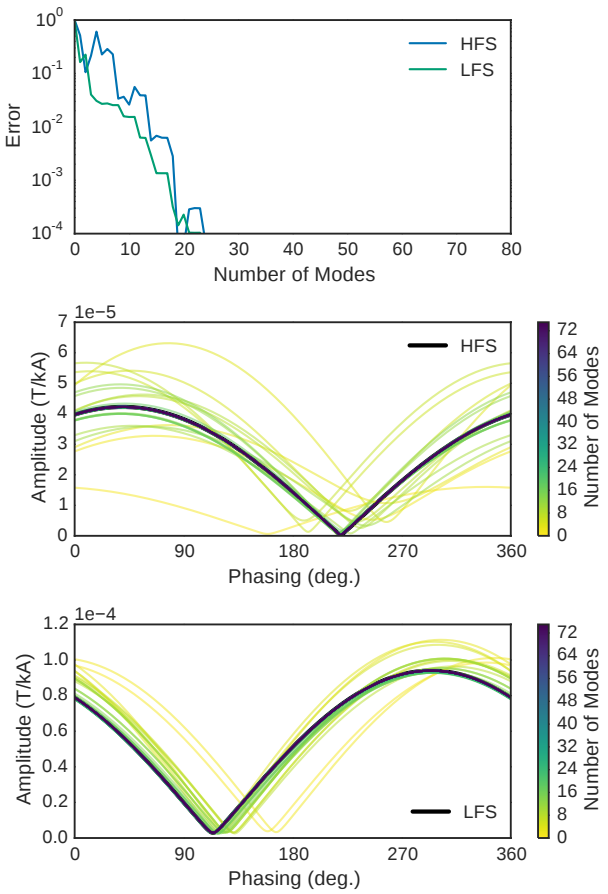

Figure 15. Top: Relative error of the HFS (blue) and LFS (green) magnetics signal produced by isolating a cumulative number of reluctance eigenmodes. Middle: The full HFS signal (black, bold) calculate by IPEC and the cumulative contributions of progressively larger numbers (indicated by color) of eigenmodes. Bottom: The corresponding full and partial signals for the LFS sensors.

mas discussed here, however, the single mode relationship provides a powerful guide to the relationship between reluctance and energy. Figure 16 shows the stability metric calculated for each reluctance eigenmode of the reference experimental equilibrium as a function of the eigenvalue normalized by the vacuum energy. The stability of the reluctance eigenmodes roughly follows the single mode curve given by Eq. (15). The reference equilibrium with β_N of 2.0 is bounded in stability between -3.5 and -0.5 and in normalized reluctance between -0.5 and 1.5. This provides the explanation for why the most sensitive modes failed to efficiently describe the plasma response: the perturbed plasma current induced by very stable modes is comparable to that of the least stable modes.

A similar plasma with higher β_N of 2.8 and L-mode β_N of 0.5 are also shown in Fig. 16. The higher pressure plasma is closer to the $n = 2$ stability boundary. Its plasma response is beginning to be dominated by the least stable, most amplifying mode. This demonstrates the convergence of these metrics near marginal stability, where single mode EF models are expected to be valid. The L-mode plasma is the most stable, and contains no larger amplification than it does shielding in terms of the normalized reluctance. This emphasizes the importance of including stable modes in the interpretation of any plasma response measured by external magnetics.

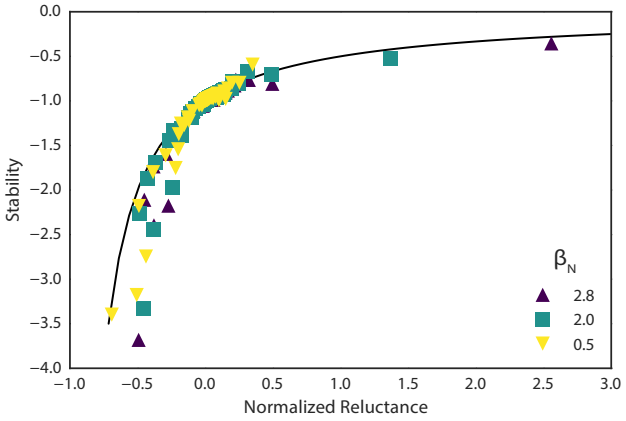

Figure 16. The stability of reluctance eigenmodes as a function of their normalized eigenvalue for the reference $\beta_N = 2.0$ equilibrium (blue, square), as well as similar $\beta_N = 2.8$ H-mode (purple, upper-triangle) and $\beta_N = 0.5$ L-mode (yellow, lower-triangle) equilibria. All points lie near the single mode trend line (black) given by Eq. (15).

No analytical definition directly relates the reluctance (or energy) eigenmodes to the IPEC RCD right singular vectors. Still, two trends can be deduced from what has been presented above. First, similar to the reluctance-energy relation, the dominant RCD mode is expected to converge with the dominant reluctance eigenmode at high β_N. Second, the stable shielding modes of the plasma response are expected to have non-negligible resonant coupling away from the single mode limit. Indeed, the resonant currents must perfectly shield the resonant perturbation at each respective rational surface in the ideal MHD equilibrium. Figure 17 confirms both of these trend are reproduced in the modeling. It shows the IPEC dominant RCD overlap metric calculated for each of the reluctance eigenmodes in the reference, high β_N, and L-mode plasmas. As expected, the total RCD is dominated by the largest reluctance mode at high β_N. At lower β_N the negative reluctance modes contain RCD overlaps on the same order as or even higher than (in the L-mode) the most positive reluctance modes. This shows that away from the $n > 1$ stability boundaries there is a class of highly stable modes that drive a significant fraction of the resonant current in the plasma. These modes can be identified in the plasma response by virtue of their large reluctance, and might be used to control RCD independent of stability.

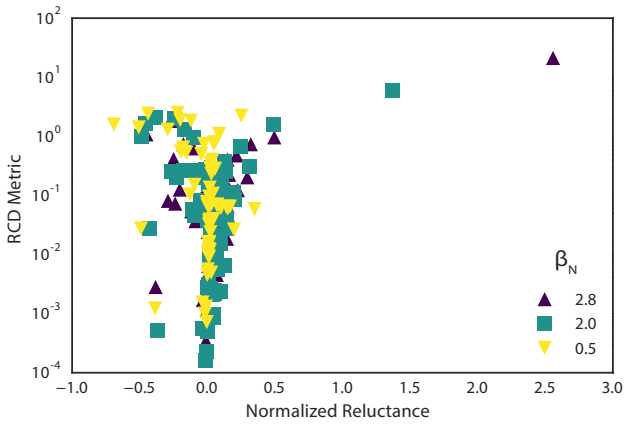

Figure 17. The IPEC dominant mode resonant current drive metric calculated of the reluctance eigenmodes as a function of their normalized eigenvalue for the reference $\beta_N = 2.0$ equilibrium (blue, square), as well as similar $\beta_N = 2.8$ H-mode (purple, upper-triangle) and $\beta_N = 0.5$ L-mode (yellow, lower-triangle) equilibria.

V. DISCUSSION AND CONCLUSIONS

The performance metrics used in single mode error field correction accurately predicted the impact of applied $n = 2$ fields in the studied plasmas, despite the multi-modal plasma response. The reference $\beta_N = 2.0$ plasma was far from the ideal MHD $n = 2$ stability boundary, and thus global instabilities were not projected to be the major impact. Indeed, the largest effects were observed to be induced pedestal transport and ELM suppression. These effects, thought to be dependent on the resonant current drive in the edge, were well correlated with the maximization of the IPEC dominant RCD mode metric. This represents a powerful continuity between the commonly single mode $n = 1$ EFC and $n > 1$ EF application for ELM suppression despite the multi-modal response and disparate consequences of the nonaxisymmetric fields.

The signals from the external magnetics, however, were not comprised of either the response to resonant drive fields or the response to the most sensitive external field structures as determined by global energy considerations. This was demonstrated in this paper by the lack of convergence or slow convergence of approximated IPEC synthetic sensor signals to the full response signal. The lack of convergence including all the resonant coupling modes showed that the magnetic sensors signals contain a significant nonresonant plasma response component. The slow, non-monotonic convergence in the energy-ranked gain basis showed that very stable modes contribute to the plasma response. This confounds the interpretation of magnetic diagnostics for possible feedback on the performance metics when the plasma is not near the stability limit for the toroidal mode number of interest (in which case, amplification of a single mode dominates). The correlation of the HFS magnetic signal with the RCD metic, for example, must be considered a coincidence of this particular case since the dominant RCD mode is responsible for only half the HFS signal.

The plasma reluctance provides a ideal MHD eigenbasis that efficiently describes both the external magnetics and the performance metrics. The reluctance is a fundamental plasma property relating external flux to the perturbed plasma current, and contains all the plasma physics requisite to describe the plasma response field external to the plasma. A small number of the largest magnitude reluctance modes can be used to approximate the measured multi-modal response. The same small number of modes have been shown to contain the least stable mode as well as the resonant coupling. This enables interpretation of the measured response in terms of the expected impact on performance.

To understand the import of these results, consider two practical applications: ELM control feedback and optimal sensor design. In the first application, the ELMs are considered to be impacted by the dominant RCD mode. A small number, $l \lesssim 10$, of reluctance eigenmodes are known to dominate the effective perturbed current. These modes are thus the only ones that external magnetics have a chance of measuring and require $l + 1$ poloidally distributed sensor arrays to constrain using the signals $\mathbf{\Phi}_d$. Feedback can then be performed on the scalar RCD metric δI_r defined as,

$$\delta I_r = \tilde{\mathbf{\Phi}}_1^{\mathcal{C}} \cdot \boldsymbol{\varrho}_l^{-1} \cdot \tilde{\mathbf{\Phi}}_d, \tag{16}$$

where $\boldsymbol{\varrho}_l^{-1}$ is the pseudo-inverse of the reluctance using the first l eigenmodes. This provides a model based parameter for feedback control of the applied 3D fields to maintain a certain level of drive for the dominant mode, resonant current in the edge, and thus ELM suppression.

This first application motivates the second, which is the optimization of sensor set design using the reluctance. A least squares fit of l basis modes using a set of poloidally distributed magnetic sensor arrays is the solution of $A \cdot x = \mathbf{\Phi}_d$ for the coefficient vector x given by multiplying both sides of the equation by the left-inverse of the basis matrix A. A common choice of basis functions are the sinusoidal bases $A_{jk} = \exp\left[i\left(n_k\phi_j - m_k\theta_j\right)\right]$, but knowledge of what responses are expected to create large fields outside the plasma would allow a more intelligent basis $A_{jk} = \tilde{\mathbf{\Phi}}_k^{\varrho}(\theta_j, \phi_j)$. The previous application provides an example of the utility of this basis. Of course, any real sensor set would have to include the mutual inductance between plasma and sensors here and in Eq. (16). Optimizing the distribution of the arrays within engineering constraints to minimize the condition number of this basis matrix would then provide the best sensor set for measuring the plasma response fields. This is beyond the scope of the current paper, but is recommended as a practical application of the new multi-modal framework developed here.

This paper identifies the multi-modal plasma response observed in DIII-D using the reluctance to interpret mag-

netic sensor signals and relate them to the physics of interest. This is a fundamentally multi-modal framework, in contrast to the single mode model EFC for which external signals were directly correlated with impact on plasma performance. With the additional complexity, however, comes new insight and opportunities for improved optimization of applied fields. The resonant current drive of very stable modes might be used, for example, to induce ELM suppression while using EFC to minimize the drive of the least stable kink. Such multifaceted EF optimization is possible when one mode is not dominating the perturbed equilibrium, and the reluctance provides the best plasma physics basis for interpreting measurements of these equilibria. Understanding how external measurements correspond to impact on plasma performance empowers optimization to maximize the benefits while minimizing the cost of 3D fields in tokamaks.

This work was supported by the U.S. Department of Energy Office of Science Office of Fusion Energy Sciences using the DIII-D National Fusion Facility, a DOE Office of Science user facility, under Awards DE-FC02-04ER54698 and DE- AC02-09CH11466. The authors are grateful to Allen Boozer for his many helpful discussions and insights. The authors also acknowledge the hard work of the entire DIII-D team, and of the Princeton collaboration at DIII-D that provided support for this work.

REFERENCES

[1] A. H. Boozer, Physical Review Letters **86**, 5059 (2001).
[2] H. Reimerdes, M. S. Chu, A. M. Garofalo, G. L. Jackson, R. J. La Haye, G. A. Navratil, M. Okabayashi, J. T. Scoville, and E. J. Strait, Physical Review Letters **93**, 135002 (2004).
[3] S. A. Sabbagh, J. Berkery, R. Bell, J. Bialek, S. Gerhardt, J. Menard, R. Betti, D. Gates, B. Hu, O. Katsuro-Hopkins, B. LeBlanc, F. Levinton, J. Manickam, K. Tritz, and H. Yuh, Nuclear Fusion **50**, 025020 (2010).
[4] J.-K. Park, M. J. Schaffer, R. J. La Haye, T. J. Scoville, and J. E. Menard, Nuclear Fusion **51**, 023003 (2011).
[5] J.-K. Park, J. E. Menard, S. P. Gerhardt, R. J. Buttery, S. A. Sabbagh, R. E. Bell, and B. P. LeBlanc, Nuclear Fusion **52**, 023004 (2012).
[6] C. Paz-Soldan, M. J. Lanctot, N. C. Logan, D. Shiraki, R. J. Buttery, J. M. Hanson, R. J. La Haye, J.-K. Park, W. M. Solomon, and E. J. Strait, Physics of Plasmas **21**, 072503 (2014).
[7] C. Paz-Soldan, R. Buttery, A. Garofalo, J. Hanson, R. La Haye, M. Lanctot, J.-K. Park, W. M. Solomon, and E. J. Strait, Nuclear Fusion **54**, 073013 (2014).
[8] E. J. Strait, R. Buttery, T. Casper, M. Chu, J. Hanson, A. Garofalo, Y. Gribov, R. La Haye, H. Reimerdes, M. J. Schaffer, and F. Volpe, Nuclear Fusion **54**, 073004 (2014).
[9] C. Paz-Soldan, N. Logan, M. Lanctot, J. Hanson, J. King, R. La Haye, R. Nazikian, J.-K. Park, and E. J. Strait, Nuclear Fusion **55**, 083012 (2015).
[10] C. Paz-Soldan, N. C. Logan, R. Haskey, S RNazikian, E. J. Strait, X. Chen, N. M. Ferraro, L. D. King, B. C. Lyons, and J.-K. Park, Nuclear Fusion - In Review (2016).
[11] A. M. Garofalo, K. H. Burrell, J. C. DeBoo, J. S. DeGrassie, G. L. Jackson, M. Lanctot, H. Reimerdes, M. J. Schaffer, W. M. Solomon, and E. J. Strait, Physical Review Letters **101**, 195005 (2008).
[12] K. H. Burrell, A. M. Garofalo, W. M. Solomon, M. E. Fenstermacher, T. H. Osborne, J.-K. Park, M. J. Schaffer, and P. B. Snyder, Physics of Plasmas **19**, 056117 (2012).
[13] A. H. Boozer, Reviews of Modern Physics **76**, 1071 (2005).
[14] A. H. Boozer, Nuclear Fusion **55**, 025001 (2015).
[15] A. H. Glasser and M. S. Chance, Bulletin American Physical Society **42**, 1848 (1997).
[16] M. Chu, M. Chance, A. Glasser, and M. Okabayashi, Nuclear Fusion **43**, 441 (2003).
[17] M. S. Chu, A. Bondeson, M. S. Chance, Y. Q. Liu, a. M. Garofalo, a. H. Glasser, G. L. Jackson, R. J. La Haye, L. L. Lao, G. a. Navratil, M. Okabayashi, H. Remierdes, J. T. Scoville, and E. J. Strait, Physics of Plasmas **11**, 2497 (2004).
[18] E. J. Strait, J. M. Bialek, I. N. Bogatu, M. S. Chance, M. S. Chu, D. H. Edgell, A. M. Garofalo, G. L. Jackson, R. J. Jayakumar, T. H. Jensen, O. Katsuro-Hopkins, J. S. Kim, R. J. La Haye, L. L. Lao, M. A. Makowski, G. A. Navratil, M. Okabayashi, H. Reimerdes, J. T. Scoville, A. D. Turnbull, and DIII-D Team, Physics of Plasmas **11**, 2505 (2004).
[19] S. A. Sabbagh, A. C. Sontag, J. Bialek, D. Gates, A. Glasser, J. Menard, W. Zhu, M. Bell, R. Bell, A. Bondeson, C. Bush, J. Callen, M. Chu, C. Hegna, S. Kaye, L. Lao, B. LeBlanc, Y. Liu, R. Maingi, D. Mueller, K. Shaing, D. Stutman, K. Tritz, and C. Zhang, Nuclear Fusion **46**, 635 (2006).
[20] J. W. Berkery, Y. Q. Liu, Z. R. Wang, S. A. Sabbagh, N. C. Logan, J.-K. Park, J. Manickam, and R. Betti, Physics of Plasmas **21**, 052505 (2014).
[21] K. C. Shaing, Physics of Fluids **26**, 3315 (1983).
[22] J.-K. Park, Physics of Plasmas **18**, 110702 (2011).
[23] N. C. Logan, J.-K. Park, K. Kim, Z. Wang, and J. W. Berkery, Physics of Plasmas **20**, 122507 (2013).
[24] K. Shaing, K. Ida, and S. A. Sabbagh, Nuclear Fusion **55**, 125001 (2015).
[25] P. B. Snyder, H. R. Wilson, J. R. Ferron, L. L. Lao, a. W. Leonard, T. H. Osborne, a. D. Turnbull, D. Mossessian, M. Murakami, and X. Q. Xu, Physics of Plasmas **9**, 2037 (2002).
[26] P. B. Snyder, T. H. Osborne, K. H. Burrell, R. J. Groebner, a. W. Leonard, R. Nazikian, D. M. Orlov, O. Schmitz, M. R. Wade, and H. R. Wilson, Physics of Plasmas **19**, 056115 (2012).
[27] N. M. Ferraro, Physics of Plasmas **19**, 056105 (2012).
[28] M. Lanctot, R. Buttery, J. de Grassie, T. Evans, N. Ferraro, J. Hanson, S. Haskey, R. Moyer, R. Nazikian, T. Osborne, D. Orlov, P. Snyder, and M. Wade, Nuclear Fusion **53**, 083019 (2013).
[29] M. Wade, R. Nazikian, J. DeGrassie, T. Evans, N. Ferraro, R. Moyer, D. Orlov, R. Buttery, M. Fenstermacher, A. Garofalo, M. Lanctot, G. McKee, T. Osborne, M. Shafer, W. M. Solomon, P. Snyder, W. Suttrop, A. Wingen, E. Unterberg, and L. Zeng, Nuclear Fusion **55**, 023002 (2015).
[30] R. Nazikian, C. Paz-Soldan, J. D. Callen, J. S. DeGrassie, D. Eldon, T. E. Evans, N. M. Ferraro, B. A. Grierson, R. J. Groebner, S. R. Haskey, C. C. Hegna, J. D. King, N. C. Logan, G. R. McKee, R. A. Moyer, M. Okabayashi, D. M. Orlov, T. H. Osborne, J.-K. Park, T. L. Rhodes, M. W. Shafer, P. B. Snyder, W. M. Solomon, E. J. Strait, and M. R. Wade, Physical Review Letters **114**, 105002 (2015).
[31] J.-K. Park, A. H. Boozer, and A. H. Glasser, Physics of Plasmas **14**, 052110 (2007).
[32] J.-K. Park, M. J. Schaffer, J. E. Menard, and A. H. Boozer, Physical Review Letters **99**, 195003 (2007).
[33] J.-K. Park, A. H. Boozer, and J. E. Menard, Physics of Plasmas **15**, 064501 (2008).
[34] A. H. Boozer, Fusion Science and Technology **59**, 561 (2011).
[35] E. J. Strait, Physics of Plasmas **22**, 021803 (2015).
[36] J. D. King, E. J. Strait, R. L. Boivin, D. Taussig, M. G. Watkins, J. M. Hanson, N. C. Logan, C. Paz-Soldan, D. C. Pace, D. Shiraki, M. J. Lanctot, R. J. La Haye, L. L. Lao, D. J. Battaglia, A. C. Sontag, S. R. Haskey, and J. G. Bak, Review of Scientific Instruments **85**, 083503 (2014).
[37] J. D. King, E. J. Strait, S. A. Lazerson, N. M. Ferraro, N. C. Logan, S. R. Haskey, J.-K. Park, J. M. Hanson, M. J. Lanctot,

Y. Liu, R. Nazikian, M. Okabayashi, C. Paz-Soldan, D. Shiraki, and A. D. Turnbull, Physics of Plasmas **22**, 072501 (2015).
[38] C. Paz-Soldan, R. Nazikian, S. R. Haskey, N. C. Logan, E. J. Strait, N. M. Ferraro, J. M. Hanson, J. D. King, M. J. Lanctot, R. A. Moyer, M. Okabayashi, J.-K. Park, M. W. Shafer, and B. J. Tobias, Physical Review Letters **114**, 105001 (2015).
[39] R. Grimm, R. Dewar, and J. Manickam, Journal of Computational Physics **49**, 94 (1983), arXiv:0021-9991(83)90116-X [10.1016].
[40] S. R. Haskey, M. J. Lanctot, Y. Q. Liu, J. M. Hanson, B. D. Blackwell, and R. Nazikian, Plasma Physics and Controlled Fusion **56**, 035005 (2014).
[41] Y. Liu, A. Kirk, and E. Nardon, Physics of Plasmas **17**, 122502 (2010).
[42] N. M. Ferraro, S. C. Jardin, and P. B. Snyder, Physics of Plasmas **17**, 102508 (2010).
[43] A. Garofalo, M. Chu, E. Fredrickson, M. Gryaznevich, T. Jensen, L. Johnson, R. L. Haye, G. Navratil, M. Okabayashi, J. T. Scoville, E. J. Strait, A. Turnbull, and D.-D. Team, Nuclear Fusion **41**, 1171 (2001).
[44] A. M. Garofalo, E. J. Strait, L. C. Johnson, R. J. La Haye, E. A. Lazarus, G. A. Navratil, M. Okabayashi, J. T. Scoville, T. S. Taylor, and A. D. Turnbull, Physical Review Letters **89**, 235001 (2002).
[45] W. A. Newcomb, Annals of Physics **10**, 232 (1960).
[46] J.-K. Park, in *57th Annual Meeting of the APS Division of Plasma Physics* (Savannah, Georgia, 2015).
[47] S. A. Lazerson, J.-K. Park, N. C. Logan, and A. Boozer, Plasma Physics and Controlled Fusion **57**, 104001 (2015).
[48] A. H. Boozer, Physics of Plasmas **10**, 1458 (2003).

PPPL PRINCETON PLASMA PHYSICS LABORATORY

Princeton Plasma Physics Laboratory
Office of Reports and Publications

Managed by
Princeton University

under contract with the
U.S. Department of Energy
(DE-AC02-09CH11466)

P.O. Box 451, Princeton, NJ 08543
Phone: 609-243-2245
Fax: 609-243-2751

E-mail: publications@pppl.gov

Website: http://www.pppl.gov